IEEE Transactions on Intelligent Transportation Systems, Available online 14 July 2025
DOI:10.1109/tits.2025.3585504

Generating G^2 continuity reference paths for autonomous vehicles at roundabouts

Qingyuan Shen, Haobin Jiang, Aoxue Li, Marco Cecotti, Chenhui Yin, You Gong

***Abstract*—Planning paths for Frenet-based autonomous vehicles (AVs) at roundabouts is difficult without complete and smooth reference paths. In such situations, the interpolating curve planner is often used to create segmented reference paths from simplified geometric roundabout data. While this method ensures curvature continuity within each curve segment, the continuity at the junctions of these segments is poor. Additionally, the determination of merging and diverging point positions at roundabouts has not been thoroughly explored. This paper introduces a novel approach using 5th-order Bézier curves to plan piecewise reference paths for AVs at roundabouts. The proposed method enhances endpoint curvature continuity of the Bézier curves and improves adaptability to non-standard roundabouts. A well-designed objective function is created to optimize both the geometric continuity parameters of the Bézier curves and the positions of merging and diverging points in the circulatory roadway. This function takes into account key factors, including path length and smoothness. Case studies validate the feasibility of maintaining curvature continuity at the endpoints and the method's ability to generalize across various scenarios, proving its effectiveness for different roundabout structures. The results also confirm the method's efficacy in generating paths from original geometric roundabout data. Lastly, the acceptable transverse deviations between real-world trajectories and reference paths demonstrate the rationality and practical applicability of this method.**

***Index Terms*—Autonomous vehicles (AVs), path planning, Roundabout, Curvature continuity, Bézier curves.**

I. Introduction

ROUNDABOUTS, serving as signal-free intersections with self-organized traffic flow, have emerged as a viable alternative to conventional intersections in many countries, particularly in Europe and North America [1]. Roundabouts offer notable benefits, including enhanced safety [2], environmental sustainability [3] and superior traffic flow management [4]. However, the inherent complexity of roundabouts presents significant challenges in path planning for autonomous vehicles (AVs), including diverse structural topologies [5], high freedom in driving behavior [6] and complex interactive negotiation behavior [7].

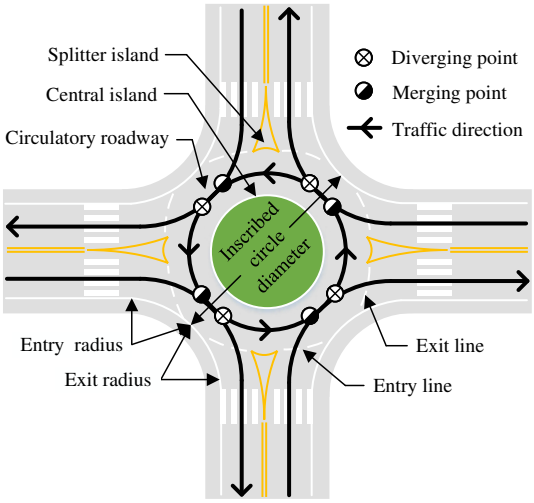

Fig. 1. Geometry elements and traffic flow characteristics at roundabouts.

Path planners for AVs typically utilize the Frenet frame as the foundational framework in algorithm development [8], [9]. These path planners impose rigorous requirements on the continuity and smoothness of the reference trajectory [10]. Simultaneously, the inherent geometric complexity of roundabouts brings increased challenges to the continuity and smoothing of the reference path. Fig. 1 shows a typical roundabout to explain its geometric attributes briefly. The key divergence between roundabouts and ordinary intersections is the presence of a central island. This feature requires vehicles to follow the circulatory roadway rather than crossing the intersection center, except for right-turn maneuvers in right-hand traffic (left-turn maneuvers in left-hand traffic). Consequently, planning a continuous and optimized path at roundabouts is significantly complicated. The planned roundabout path must undergo multiple curvature changes at both diverging and merging points in the circulatory roadway [11], [12]. Therefore, developing a path-smoothing algorithm specifically tailored for roundabouts incurs increased computational costs

Manuscript received October 18, 2023. The work was supported by the National Natural Science Foundations of China (No. 52202414), the Project of Philosophy and Social Science Research in Colleges and Universities in Jiangsu Province (2022SJYB2207), Public Open Project of Automobile Standardization (CATARC-Z-2024-00116), two Postgraduate Research & Practice Innovation Program of Jiangsu Province (No. KYCX22_3618 and No. KYCX21_3334). This work was also partially supported by the Department of Xiamen Human Resources and Social Security under grant number 12024008. Map data is copyrighted by OpenStreetMap contributors and available from https://www.openstreetmap.org. (Corresponding authors: Haobin Jiang and Aoxue Li.)

Qingyuan Shen and Aoxue Li are with the School of Automotive and Traffic Engineering, Jiangsu University, Zhenjiang 212013, China (e-mail: qingyuanshen@stmail.ujs.edu.cn; liax@ujs.edu.cn)

Haobin Jiang is with Automotive Engineering Research Institute, Jiangsu University, Zhenjiang 212013, China (e-mail: jianghb@ujs.edu.cn)

Marco Cecotti and Chenhui Yin are with the School of Aerospace, Transport and Manufacturing, Cranfield University, Cranfield, MK43 0AL, U.K. (e-mail: M.cecotti@cranfield.ac.uk; Chenhui.Yin@cranfield.ac.uk)

You Gong is with the School of Mechanical and Automotive Engineering, Xiamen University of Technology, Xiamen 361024, China (e-mail: 2024100023@xmut.edu.cn)

TABLE I
COMPARISON OF THE INTERPOLATING CURVE PLANNERS AT ROUNDABOUTS.

Papers	Smooth	Continuity	Merging/diverging point decision
Pérez et al. (2011) [14]	N/A	G^0	N/A
Rubio-Martín et al. (2019) [15]	Line&circle	G^1	Tangent points of entrance/exit arc and circle
Silva and Grassi (2017) [12]	Clothoids	G^2	Semi-empirical function (pre-defined radius and angle offsets)
Pérez et al. [16] & Rastelli and Peñas (2015) [17]	3rd-order Bézier	G^1	Semi-empirical function (pre-defined distance away from the junction point)
González and Pérez (2013) [18] & González et al. (2017) [13]	3rd/4th-order Bézier	G^1	Semi-empirical function (pre-defined distance from the roundabout center and the previous/next intersection)
Lattarulo et al. (2018) [19] & Hidalgo et al. (2019) [20]	4th-order Bézier	G^2	Empirical value (the distance from the circle to the entrance/exit)
Hsu and Liu (2020) [21]	Hybrid (η^3 spline and Bézier)	G^3	Empirical value
Cao and Zoldy (2022) [22]	B-spline	G^2	Selected by the octant points of the circle
Proposed	5th-order Bézier	G^2	Cost function of the path's length and smoothness improved by Genetic Algorithm (GA)

to achieve a similar level of smoothness as planned paths for ordinary intersections [13].

To date, the research community has proposed various methodologies to plan reference paths for roundabouts, summarized in Table I. In 2011, Pérez et al. [14] pioneered the research domain of AV roundabout reference path planning. This study simplified the characteristics of roundabout paths using a parametric equation for a circular trajectory. However, it did not focus on path smoothing, resulting in reference paths with poor smoothness. These inadequately smoothed paths can lead to critical tracking errors and diminished ride quality for autonomous vehicles (AVs) [23], [24]. To enhance the smoothness of planned paths at roundabouts, various smoothing approaches using interpolating curve planners have been introduced. Meanwhile, the kth-order geometric continuity concept, denoted as G^k continuity, was introduced as a pivotal metric for assessing path smoothness [25]. For instance, Rubio-Martín et al. [15] investigated smooth paths composed of tangents and circular arcs. Despite the relative simplicity in the geometric construction of these paths, they achieved only G^1 continuity at the connection points of lines and circles. The absence of G^2 continuity in such paths negatively impacts path-tracking accuracy and passenger comfort.

Several parameterizable curve styles have been investigated as potential candidates for achieving high-order geometric continuity in roundabout path planning [26]–[28]. The clothoid curve has been considered by [12] due to its ability to smoothly connect circular arcs and straight-line segments. However, the computational complexity of the clothoid curve makes it unsuitable for real-time applications [24]. Among available curve styles, the Bézier curve is a prominent choice. Bézier curves are parametric curves defined by control points, featuring closed-form expressions and intuitive parameter selection. They are widely used in roundabout path planning [12], [13], [16]–[20]. Typically, 3rd/4th-order Bézier curves are employed to smooth paths requiring attaining G^2 continuity. This choice is based on the understanding that curves of an order lower than the third cannot adequately meet the demands of continuity and curvature boundedness. Despite these efforts, existing research has not yet delved into optimizing G^2 continuity at diverging and merging points.

Moreover, Hsu and Liu [21] proposed a hybrid method combining η^3 spline curves with 7th-order Bézier curves to improve passenger comfort. They evaluated the path's smoothness, ensuring low sharpness. However, this study did not explicitly address continuity issues at diverging and merging points. Additionally, although Bézier curves of seven or higher order can minimize snap, they become more prone to oscillations and harder to control as the order increases, requiring more computational resources [29]. These complexities can pose limitations in their practical application. Conversely, Cao et al. [22] introduced an alternative approach using uniform cubic B-spline curves constructed from collected waypoints and octant points of circles. However, this method may have limitations when applied to non-standard roundabouts. It's noteworthy that employing B-spline curves can increase computational costs due to their relatively complex mathematical formulations, despite their advantages in local controllability compared to Bézier curves [30].

In addition to traditional planning methods based on fitting interpolation curves, numerical optimization methods play a crucial role in generating continuous paths for AVs. Path planning methods based on numerical optimization typically calculate trajectories according to kinematic constraints or smooth previously calculated trajectories [31], [32]. They fully consider different constraints and enrich performance objectives. Chai et al. [33] presented a multi-objective trajectory optimization framework for unmanned ground vehicles (UGVs) in first aid scenarios. The method focuses on balancing multiple objectives, such as minimizing travel time and ensuring safety, which are also key considerations for roundabout navigation. Additionally, parameters such as position, velocity, acceleration and jerk are crucial factors for planning. A high-order continuous trajectory can be obtained by optimizing a function when the mobile robot is in a narrow channel or avoiding obstacles [34], [35]. However, path planning methods based on numerical optimization often require shifting the original discrete points to achieve the optimization goal, reducing their representation's accuracy. Additionally, function optimization for each motion state is very time-consuming, requiring the entire process to be completed within a given time frame.

Simultaneously, with the rapid development of machine learning, motion planning methods with self-learning capa-

bilities have become a significant research direction. Deep Learning (DL) and Reinforcement Learning (RL) techniques are regarded as the most suitable methods for solving motion planning problems in unknown dynamic environments [36], [37]. The robot motion planning approach using Deep Reinforcement Learning (DRL) enhances the robot's policy by interacting with the surrounding environment. Robots employing this approach could potentially acquire a resilient capacity for autonomous learning and decision-making. This capacity plays a pivotal role in navigating unstructured environments, such as partially mapped and dynamically changing surroundings [38]. Although reinforcement learning-based path planning technology has been applied in some scenarios, challenges and difficulties remain. For example, the stability and convergence of the algorithm, the difficulty in selecting hyperparameters, and the interpretability and generalization of the model need further research and exploration [38].

In summary, most research groups commonly utilize interpolation to address planning challenges. The primary rationale for selecting this approach is the ability of an improved map within structured settings to provide the requisite waypoints, such as GPS data. Consequently, optimal trajectories characterized by smoothness, continuity, vehicle limitations, speed and comfort are produced [8]. Although prior studies have conducted in-depth research on the smoothness of paths, each method has some problems to a greater or lesser extent. For example, paths generated by tangents and arcs are discontinuous, leading to jerky transitions between segments. Clothoids are computationally intensive due to the need for curve integration. Additionally, while the curvature of the clothoid is continuous, it follows a linear behavior that is not smooth enough. For paths with fixed boundary positions, directions, and curvatures, it is often impossible to generate a clothoid curve. Although 3rd and 4th-order Bézier curves can achieve continuous curvature, they cannot ensure curvature continuity at the joints of segmented curves. Although B-spline curves offer better local controllability than Bézier curves, their complex mathematical formulations and increased number of parameters can lead to higher computational costs. Additionally, polynomial curves are another conventional interpolation method. However, due to the limited expressiveness of polynomial curves, they cannot accurately fit conic sections (such as arcs and ellipses), which are often the shape of the central island. Therefore, polynomial curves are not suitable for roundabout path planning. Ultimately, this paper chose to use the 5th-order Bézier curve method. The Bézier curve is a parametric curve defined by control points and a closed-form expression. Thus, it offers advantages such as high flexibility, intuitive parameter selection, and computational efficiency. It is the most widely used curve-fitting algorithm for path planning [39], [40].

Meanwhile, previous studies have paid limited attention to the merging and diverging points of roundabouts. Specifically, the continuity of these points has not been incorporated into path evaluation processes. The absence of G^2 continuity at these pivotal points can significantly impede passenger comfort and tracking performance. Furthermore, past studies have typically employed empirical values, semi-empirical functions and predefined methodologies to determine the locations of merging and diverging points. However, these approaches tend to falter when confronted with complex roundabout structures and unsimplified geometric data. With this regard, this study aims to propose an innovative roundabout reference path planning approach based on 5th-order Bézier curves. This framework aims to optimize the planned path and address the challenge of merging and diverging points, ensuring the continuity of the entire path, even with complicated roundabout structures and unsimplified geometric data.

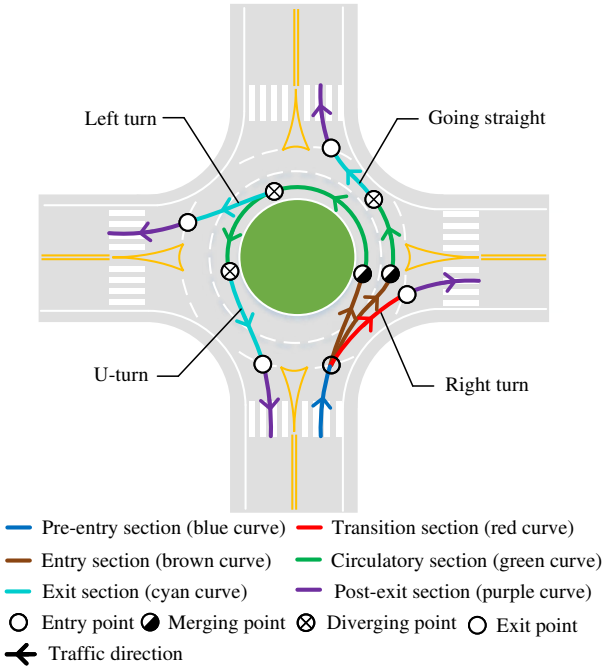

Fig. 2. Reference path sections and their joint points at the roundabout.

The contributions of this study are as follows:

1) A reference path planning approach specifically tailored for roundabouts is proposed. This approach leverages 5th-order Bézier curves to govern the G^2 continuity of connection points, and the length and smoothness of the path are optimized by a proper objective function.
2) The presented planning algorithm facilitates the utilization of geometric roundabout data without simplification, eliminating the need for simplification steps typically required in roundabout path planning.

The rest of this paper is organized as follows: Section II presents the methods for generating reference paths with 5th-order Bézier curves in different sections and achieving G^2 continuity at meeting points of different curves. Section III details the corresponding mathematical model. Section IV shows the simulation of reference path generation and analyses the distribution of natural driving trajectories to verify the feasibility and effectiveness of the algorithm proposed in this study. Conclusions and outlooks are presented in Section V.

II. Description of Reference Path Planning

Fig. 2 illustrates reference paths within a standard roundabout for various driving directions. The path generation pro-

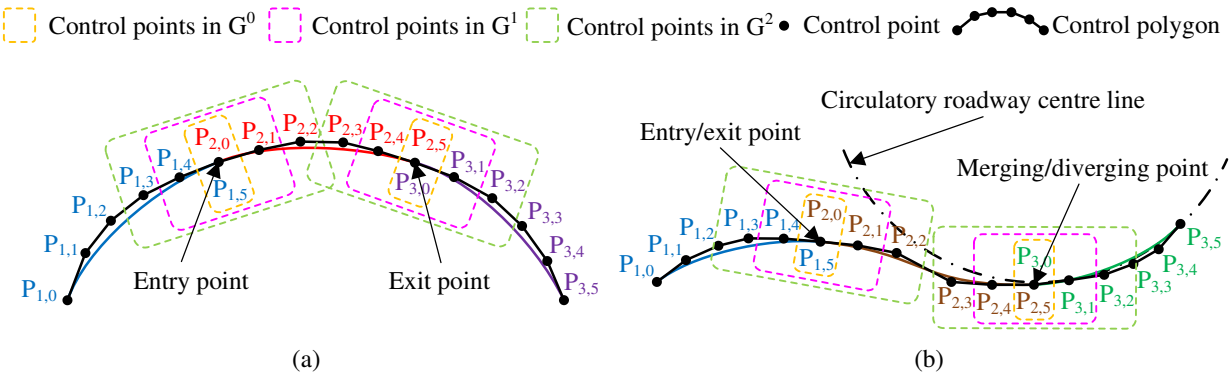

Fig. 3. The generation methods of the 5th-order Bézier curve for (a) the transition section and (b) entry and exit sections at the roundabout. The entry point $P_{2,0}$ and exit point $P_{2,5}$ in (a) correspond to the entry and exit points of the transition section in Fig. 2, respectively. The entry point $P_{2,0}$ and exit point $P_{2,5}$ in (b) correspond to the merging and diverging points of the entry/exit section in Fig. 2, respectively. The determination of control points $P_{2,0}$ and $P_{2,5}$ involves achieving G^0 continuity, $P_{2,1}$ and $P_{2,4}$ are associated with G^1 continuity, while $P_{2,2}$ and $P_{2,3}$ pertain to G^2 continuity.

cess is considerably more complex than at conventional crossroads, as these paths must adhere to the circulatory roadway while navigating the roundabout. To manage the complexity of roundabouts, a complete reference path is divided into several distinct sections. Roundabouts usually feature lane lines in the pre-entry, circulatory roadway and post-exit zones, which are used to create corresponding reference paths for these sections. Sections equipped with lane lines for reference conduct Bézier curve calculations by fitting discrete points extracted from the lane center line. Furthermore, formulating the complete reference path requires planning the entry and exit sections to connect seamlessly. Notably, entry and exit sections lack lane lines as references for path generation. Additionally, the right-turn path comprises only the pre-entry, transition and post-exit sections (as the central island has a relatively minor influence on this path, particularly in mini or small roundabouts). The transition section of the right-turn path also lacks lane lines for reference [41]. Sections without reference lane lines, including entry, exit and transition sections, must compute Bézier curves based on high-order continuity conditions, considering the Bézier curves on both sides to ensure the smoothness of the entire reference path.

Fig. 3 clearly demonstrates the proposed method for generating Bézier curves in various sections and the control points involved in different geometric continuity constraints (G^0, G^1 and G^2). The relevant theoretical proof can be derived from [42]. Herein, $P_{a,b}$ denotes the control point, with 'a' taking values from 1 to 3, representing three distinct curves, and 'b' ranging from 0 to 5, representing the six control points for each Bézier curve. The line segments $P_{a,0}$ to $P_{a,1}$, $P_{a,1}$ to $P_{a,2}$, and so forth up to $P_{a,b-1}$ to $P_{a,b}$ are referred to as "leg", and when joined sequentially, they form a control polygon. Fig. 3(a) illustrates the generation of all Bézier curves for right-turn scenarios without the circulation section. This involves the pre-entry ($a = 1$), transition ($a = 2$) and post-exit sections ($a = 3$) with fixed connection points between these sections, i.e., entry and exit points. Control points for the pre-entry section $P_{1,b}$ and post-exit section $P_{3,b}$ are determined by fitting lane center discrete points. Control points for the transition section $P_{2,b}$ are further computed in accordance with G^0, G^1 and G^2 continuity with adjacent Bézier curves. Further details regarding the specific formula derivation can be found in Section III.

Fig. 3(b) depicts the Bézier curve generation method for other driving directions within a roundabout. When a vehicle enters a roundabout, the planned reference path comprises pre-entry ($a = 1$), entry ($a = 2$) and circulatory sections ($a = 3$). When exiting the roundabout, the reference path includes post-exit ($a = 1$), exit ($a = 2$) and circulatory sections ($a = 3$). Similarly, control points $P_{1,b}$ and $P_{3,b}$ are obtained by fitting lane center discrete points, while $P_{2,b}$ is determined based on G^0, G^1 and G^2 continuity with other Bézier curves. Nevertheless, the positions of the merging and diverging points in Fig. 3(b) can move along the circulatory roadway center line rather than being fixed points. These points need to be further optimized to ensure the overall smoothness of the reference path. In response, this study introduces an appropriate cost function to determine optimal locations for merging and diverging points. The evaluation criteria involve path length and smoothness of the reference path.

In summary, the path planner initially divides the roundabout path into discrete sections based on structural parameters and driving direction. Subsequently, the reference path is generated by leveraging lane line data within the roundabout and adhering to G^0, G^1 and G^2 continuity principles. The mathematical modeling and corresponding cost function for the path planner will be explained in the following section.

III. Mathematical Modeling

The detailed steps for calculating the control points of curves 1, 2 and 3 are as follows.

Firstly, the sections within the reference path are modeled using the standard 5th-order Bézier curve. The equation is depicted as follows [43]:

$$P_a(u) = \sum_{i=0}^{5} P_{a,i} B_{i,n}(u) \quad u \in [0,1], \tag{1}$$

where

$$B_{i,n}(u) = \frac{n!}{(n-i)!i!} u^i (1-u)^{n-i}. \tag{2}$$

Here, $P_a(u)$ represents the 5th-order Bézier curve. $P_{a,i}$ (i = 0, 1, 2, ..., 5) are the 6 control points for Bézier curve a ($a = 1, 3$). The input of this function $u \in [0, 1]$ is a proportion determining the position from start to end points. $B_{i,n}(u)$ is a Bernstein polynomial of the nth-order Bézier curve ($n = 5$ for the 5th-order Bézier curve).

In detail, the discrete points of the lane center line $P_a(U)$, control points P_a and their corresponding Bernstein polynomial B are represented by vectors as follows to explain conveniently:

$$\begin{aligned} P_a(U) &= [P_a(u_0) \quad P_a(u_1) \quad \cdots P_a(u_m)]^T \\ P_a &= [P_{a,0} \quad P_{a,1} \quad \cdots P_{a,5}]^T \\ B &= \begin{bmatrix} B_{0,5}(u_0) & B_{1,5}(u_0) & \cdots & B_{5,5}(u_0) \\ B_{0,5}(u_1) & B_{1,5}(u_1) & \cdots & B_{5,5}(u_1) \\ \cdots & \cdots & \cdots & \cdots \\ B_{0,5}(u_m) & B_{1,5}(u_m) & \cdots & B_{5,5}(u_m) \end{bmatrix}. \end{aligned}$$

Since the discrete points of the lane center line $P_a(U)$ obtained from the real world have errors, the control points P_a are calculated by the least-squares method:

$$P_a = \left(B^T B\right)^{-1} B^T P_a(U). \tag{3}$$

Therefore, the Bézier curve $P_a(U)$ ($a = 1, 3$) can be obtained by substituting the control points P_a into Eq.1. Then, curve 2 can be computed using G^0, G^1 and G^2 continuity with curves 1 and 3.

Secondly, according to the endpoint interpolation of the Bézier curve, if curve 2 has G^0 continuity with curves 1 and curve 3, control points $P_{1,5}$, $P_{2,0}$, $P_{3,0}$ and $P_{2,5}$ must coincide to ensure position continuity:

$$\begin{cases} P_{2,0} = P_{1,5} \\ P_{2,5} = P_{3,0}. \end{cases} \tag{4}$$

Thirdly, according to the endpoint tangent of the Bézier curve, if curve 2 meets G^1 continuity with curves 1 and 3, in addition to satisfying G^0 continuity, the first derivatives of control points $P_{2,0}$, $P_{1,5}$, $P_{2,5}$ and $P_{3,0}$ must satisfy the following conditions:

$$\begin{cases} P'_{2,0} = \alpha_{1,2} P'_{1,5} \\ P'_{2,5} = \alpha_{2,3} P'_{3,0}, \end{cases} \tag{5}$$

where $\alpha_{1,2}$ and $\alpha_{2,3}$ are arbitrary positive constants.

Among them, the first derivative $P'_a(u)$ of $P(u)$ are described as follow:

$$P'_a(u) = n \sum_{i=0}^{n-1} \left(P_{a,i+1} - P_{a,i}\right) B_{i,n-1}(u), \tag{6}$$

where the first derivatives of the meeting point of curves 1, 2 and 3 are expressed as follows:

$$P'_{2,0} = 5(P_{2,1} - P_{2,0}) \tag{7}$$

$$P'_{1,5} = 5(P_{1,5} - P_{1,4}) \tag{8}$$

$$P'_{2,5} = 5(P_{2,5} - P_{2,4}) \tag{9}$$

$$P'_{3,0} = 5(P_{3,1} - P_{3,0}). \tag{10}$$

By substituting Eqs. 4, 7, 8, 9, 10 into Eq.5 yields:

$$\begin{cases} P_{2,1} = \alpha_{1,2}(P_{1,5} - P_{1,4}) + P_{1,5} \\ P_{2,4} = -\alpha_{2,3}(P_{3,1} - P_{3,0}) + P_{3,0}, \end{cases} \tag{11}$$

where $P_{2,1}$ and $P_{2,4}$ can be calculated by adjusting the value of $\alpha_{1,2}$ and $\alpha_{2,3}$.

Fourthly, if curve 2 achieves G^2 continuity with curves 1 and 3 at the endpoints, in addition to satisfying G^0 and G^1 continuity, the second derivatives at the meeting points of curves 1, 2 and 3 must also satisfy the following condition:

$$\begin{cases} P''_{2,0} = \alpha_{1,2}^2 P''_{1,5} + \beta_{1,2} P'_{1,5} \\ P''_{2,5} = \alpha_{2,3}^2 P''_{3,0} + \beta_{2,3} P'_{3,0}, \end{cases} \tag{12}$$

where $\beta_{1,2}$ and $\beta_{2,3}$ are arbitrary constants.

Among them, the second derivative $P''_a(u)$ of $P(u)$ are described as the following equations:

$$P''_a(u) = n(n-1) \sum_{i=0}^{n-2} \left(P_{a,i+2} - 2P_{a,i+1} + P_{a,i}\right) B_{i,n-2}(u), \tag{13}$$

where the second derivatives of control points $P_{2,0}$, $P_{1,5}$, $P_{2,5}$ and $P_{3,0}$ are expressed as follows:

$$P''_{2,0} = 20(P_{2,2} - 2P_{2,1} + P_{2,0}) \tag{14}$$

$$P''_{1,5} = 20(P_{1,5} - 2P_{1,4} + P_{1,3}) \tag{15}$$

$$P''_{2,5} = 20(P_{2,5} - 2P_{2,4} + P_{2,3}) \tag{16}$$

$$P''_{3,0} = 20(P_{3,2} - 2P_{3,1} + P_{3,0}). \tag{17}$$

By substituting Eqs.4, 11, 14, 15, 16, 17 into Eq.12 yields:

$$\begin{cases} P_{2,2} = & \alpha_{1,2}^2 (P_{1,5} - 2P_{1,4} + P_{1,3}) \\ & + \left(2\alpha_{1,2} + \frac{\beta_{1,2}}{4}\right)(P_{1,5} - P_{1,4}) + P_{1,5} \\ P_{2,3} = & \alpha_{2,3}^2 (P_{3,2} - 2P_{3,1} + P_{3,0}) \\ & - \left(2\alpha_{2,3} - \frac{\beta_{2,3}}{4}\right)(P_{3,1} - P_{3,0}) + P_{3,0}, \end{cases} \tag{18}$$

where $P_{2,2}$ and $P_{2,3}$ can be calculated by adjusting the value of $\alpha_{1,2}$, $\alpha_{2,3}$, $\beta_{1,2}$ and $\beta_{2,3}$.

As a result, all control points of curve 2 in Fig. 3(a) can be found as follows: the control points $P_{2,0}$ and $P_{2,5}$ can be determined by the Eq.4; the control points $P_{2,1}$, $P_{2,2}$, $P_{2,3}$ and $P_{2,4}$ can be computed by adjusting $\alpha_{1,2}$, $\alpha_{2,3}$, $\beta_{1,2}$ and $\beta_{2,3}$ according to Eqs.11 and 18. Finally, the Bézier curve $P_a(U)$ ($a = 2$) can be determined by substituting the control points $P_{2,b}$ into Eq.1.

Additionally, unlike in Fig. 3(a), the merging point $P_{2,5}$ of curve 2 in Fig. 3(b) still needs to be optimized. Overall, curve 2 is shaped by $\alpha_{1,2}$, $\alpha_{2,3}$, $\beta_{1,2}$, $\beta_{2,3}$ and the merging point $P_{2,5}$. These proportional coefficients ($\alpha_{1,2}$, $\alpha_{2,3}$, $\beta_{1,2}$, $\beta_{2,3}$) have countless theoretical solutions. However, for the application scenarios in this study, these undetermined coefficients can be determined by a cost function that considers the trade-off of two parameters: the length and smoothness of the reference path. These two parameters are key indicators for evaluating an ideal path [44], [45].

Fifthly, the reference path length is primarily influenced by the merging point's position. The driver's primary task when

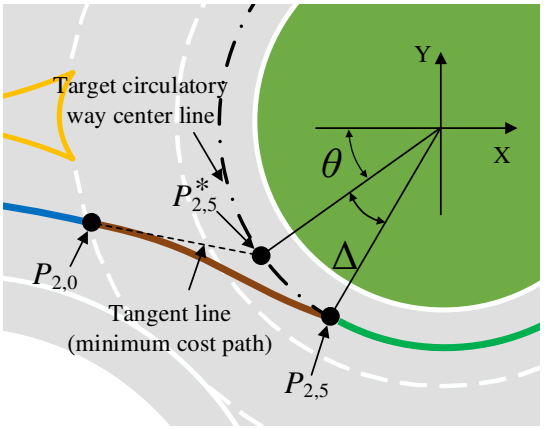

Fig. 4. $P_{2,5}$ search algorithm based on the Frenet coordinate system, where θ and Δ are the iterative initial angle and the certain search angle, respectively.

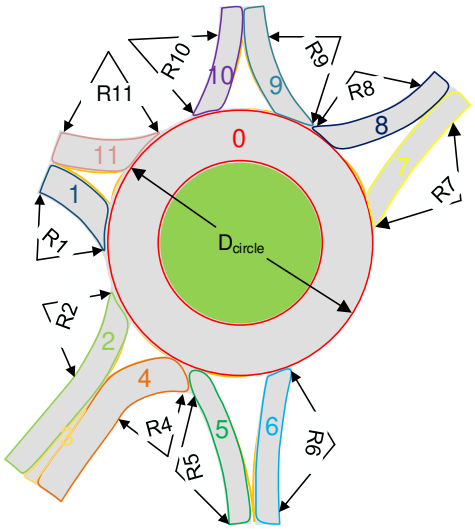

Fig. 5. Geometric parameter characteristics and entrance (#1, #4, #6, #8, #10) and exit (#2, #5, #7, #9, #11) labels of Roundabout (A) in CitySim data set

entering the roundabout is to merge safely with the circulatory traffic. However, if the driver turns the steering wheel in the opposite direction to shorten the merging distance, the relative heading angle between the merging and circulating vehicles increases, raising the collision risk and hindering a safe merging process. Therefore, this paper argues that maintaining the heading angle at the yield line while entering the circulatory roadway represents the minimum cost merging distance, disregarding the smoothness of the merging point. Additionally, to ensure the smoothness of the merging point, it is necessary to extend the merging distance appropriately. Thus, the ideal path balances smoothness requirements with a slight increase in merging distance, aligning with human driver needs.

Therefore, the ideal merging point is assumed to be on the center line of the target circulatory roadway. Hence, the merging point $P_{2,5}$ should be searched along the center line of the target circulatory roadway in the same direction as the traffic flow. To simplify the search scope, a global coordinate system for the roundabout is created based on the Cartesian

TABLE II
THE DETAIL PARAMETERS OF ROUNDABOUT (A) IN CITYSIM DATA SET

Category	Non-standard, Single-Lane
Inscribed circle diameter	#0:$\sim 37m$
Circulatory road width	#0:$\sim 6.57m$
Entry radius	#1:$\sim 18.4m$ #4:$\sim 15.5m$ #6:$\sim 20.5m$ #8:$\sim 17.2m$ #10:$\sim 16.5m$
Exit radius	#2:$\sim 11.0m$ #5:$\sim 29.5m$ #7:$\sim 38.2m$ #9:$\sim 20.4m$ #11:$\sim 25.7m$

coordinate system in Fig. 4, with the roundabout's center is the coordinate system's origin. One of the search boundary points $P^*_{2,5}$ is the cross point of the tangent line of $P_{2,0}$ on curve 2 and the target circulatory center line. $P^*_{2,5}$ is where the vehicle maintains its current heading to pass the entrance line and drives nearest to the target circular lane center line. Therefore, the segment from $P_{2,0}$ to $P^*_{2,5}$ is called the minimum cost path. Specifically, the angle between the line from $P^*_{2,5}$ to the origin of the coordinate system and the X-axis is the iterative initial angle θ. Starting from the search point $P^*_{2,5}$, a certain search angle $\Delta \in [0, \pi/2]$ is applied to find a new $P_{2,5}$ on the target circulatory center line, which is another search boundary. Furthermore, to improve the search speed of the optimization algorithm, the length of the first leg of curve 2 is assumed to be part of the last leg of curve 1, and the length of the last leg of curve 2 is part of the first leg of curve 3, with the parameter domain of $\alpha_{1,2}, \alpha_{2,3} \in (0, 1)$.

Sixthly, although the values of the geometric continuity scale parameters $\alpha_{1,2}$, $\alpha_{2,3}$, $\beta_{1,2}$, $\beta_{2,3}$ do not affect the continuity at the merging and diverging points, they will lead to the deterioration of the higher-order smoothness (fairness) of the path. Specifically, an ideal path not only needs to maintain curvature continuity but also requires good fairness [46], which is often overlooked in previous roundabout path planning research. Fairness is often associated with the aesthetics and functional smoothness of a curve, but translating it into mathematical terms is complex [43]. Although there is no consensus in the academic community on the exact definition of the concept of fairness, it is generally believed that curvature is a key indicator for evaluating the fairness of a curve [47], [48]. Therefore, combined with this research scenario, three evaluation indicators considering the fairness of the reference path are established: $K_{peak}, K'_{peak}, K''_{peak}$, which take into account both the local characteristics of the curve and the global issues.

In summary, a suitable cost function is proposed to optimize the proportional coefficients and the merging/diverging point to achieve an ideal overall reference path. The cost function considers two critical indicators for transition path generation: length and smoothness. Four evaluation indicators for reference path generation are established as follows:

$$\begin{cases} L_{relative} = |l_{real} - l_{miniCost}| \\ K_{peak} = \sum |k_{peak}| \\ K'_{peak} = \sum |k'_{peak}| \\ K''_{peak} = \sum |k''_{peak}|, \end{cases} \tag{19}$$

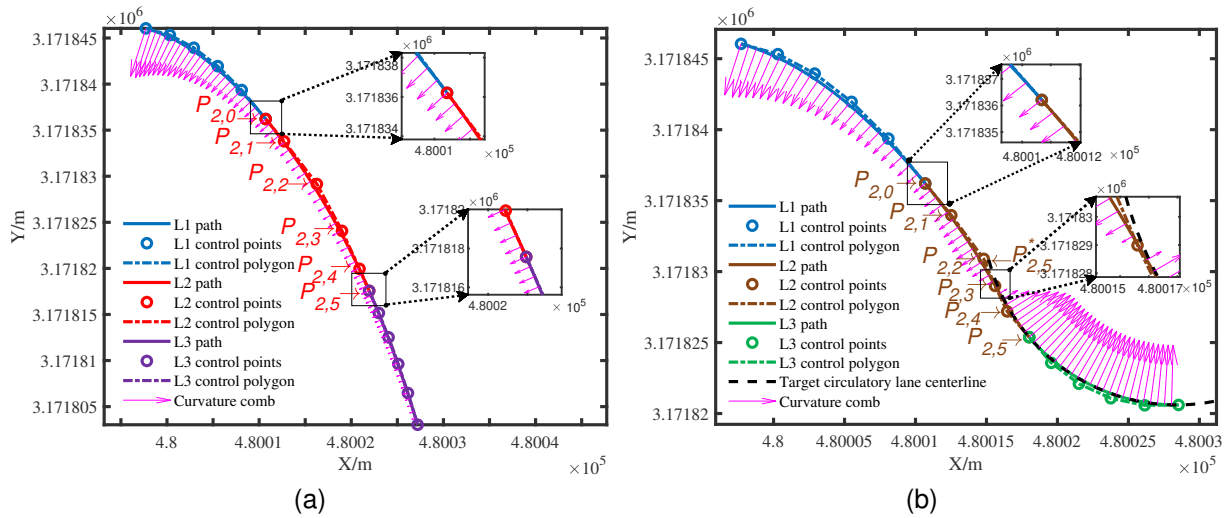

Fig. 6. The characteristics of the planned piecewise Bézier reference paths (L1, L2 and L3) in the right turn scenario (a) and entry scenario (b), including reference paths, control points, control polygons and curvature combs.

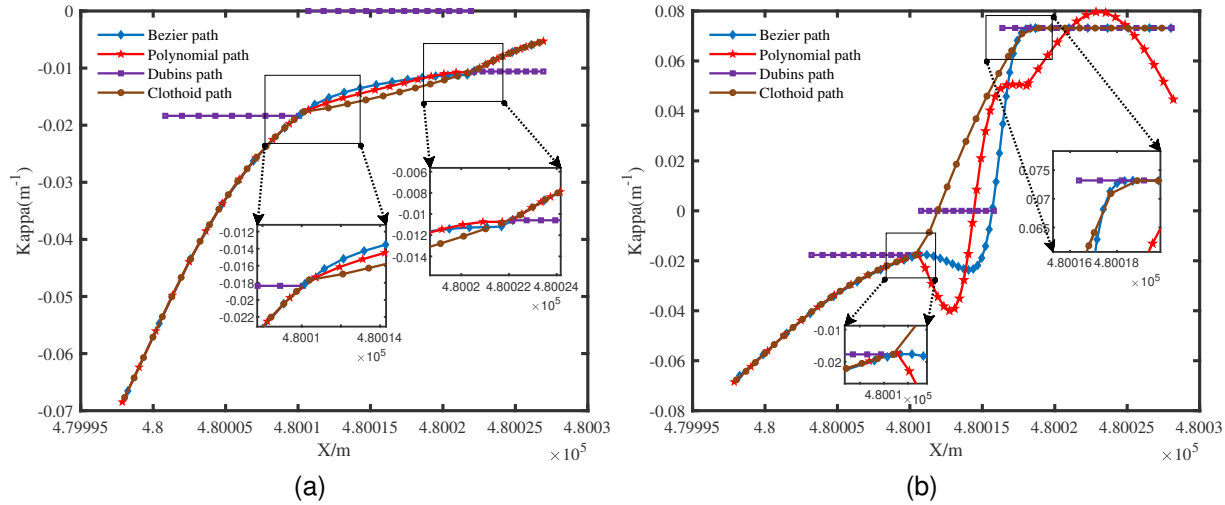

Fig. 7. Curvature profiles of L1, L2, and L3 reference paths generated by different interpolation curve methods in the right-turn scenario (a) and the entering scenario (b).

where the relative path length $L_{relative}$ is the difference in length between the real path l_{real} and the minimum cost path $l_{miniCost}$; K_{peak} is the total absolute value of the path's curvature peak (k_{peak}); K'_{peak} is the total absolute value of the path's curvature derivative peaks (k'_{peak}); K''_{peak} is the total absolute value of the path's second derivative of the curvature peaks (k''_{peak}). The above four parameters are related to $\alpha_{1,2}$, $\alpha_{2,3}$, $\beta_{1,2}$, $\beta_{2,3}$ and $P_{2,5}$. Minimum cost path $l_{miniCost}$ is related to points $P_{2,0}$ and $P^*_{2,5}$.

Seventhly, to make the cost function simple and efficient to calculate, the four evaluation indicators were combined into a composite evaluation indicator using the weighted sum model (WSM), with weights assigned objectively and rationally by the entropy weight method (EWM). The cost function is defined as follows:

$$\begin{aligned}\min(h) =&\mathrm{W}_{relativeL} * L_{relative} + \mathrm{W}_{peakK} * K_{peak} \\ &+\mathrm{W}_{peakK'} * K'_{peak} + \mathrm{W}_{peakK''} * K''_{peak}.\end{aligned} \tag{20}$$

Meanwhile, due to the limitations of the mechanical steering system and the motion comfort of a vehicle, the curvature k and the curvature rate k' are bounded as follows:

$$\begin{cases} |k| \le k_{max} \\ |k'| \le \sigma_{max}, \end{cases} \tag{21}$$

where $\kappa_{max} = 1/\rho_{min}$, with ρ_{min} being the minimum turning radius, and σ_{max} is the maximum curvature rate as one of the comfort index.

Overall, the cost function is subject to the following constraints:

$$\begin{cases} 0 < \alpha_{1,2} < 1 \\ 0 < \alpha_{2,3} < 1 \\ 0 \le \Delta \le \frac{\pi}{2} \\ |k| \le k_{\max} \\ |k'| \le \sigma_{\max}. \end{cases} \tag{22}$$

Finally, a genetic algorithm (GA) is applied to search for the geometric continuous scale parameters ($\alpha_{1,2}$, $\alpha_{2,3}$, $\beta_{1,2}$, $\beta_{2,3}$) and the location of merging points $P_{2,5}$ to improve the solving

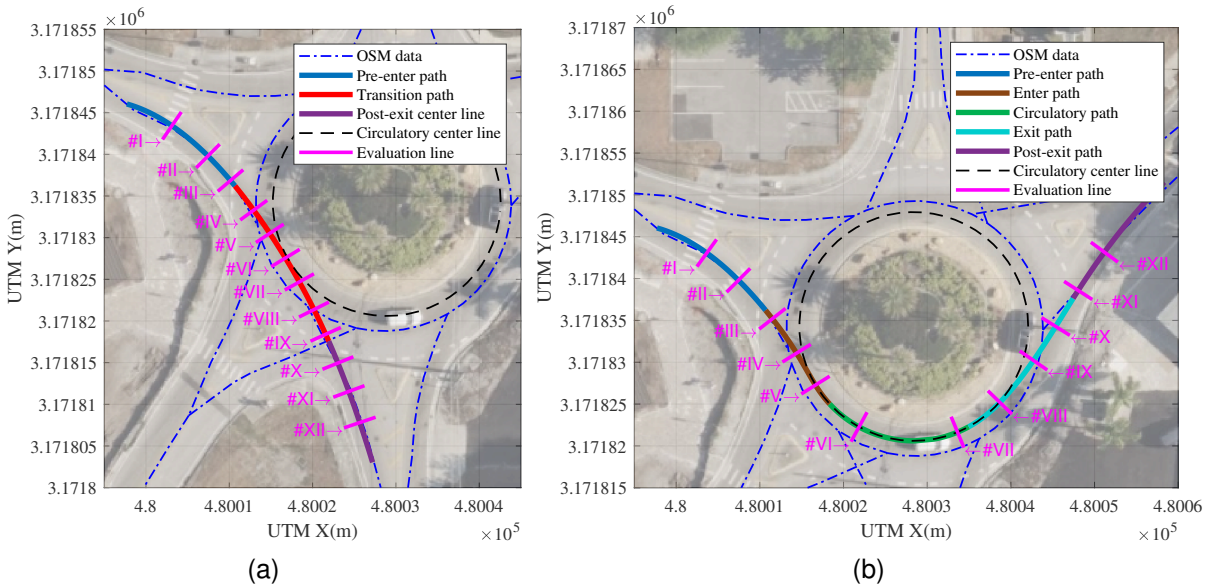

Fig. 8. The distribution of the evaluation lines on the reference paths of the Lane ID #1-#5 (a) and Lane ID #1-#7 (b) at Roundabout (A).

performance of this nonlinear cost function. The number of design variables is 5, the population size is 50, the population type is a double vector, the crossover function is "constraint dependent", the mutation function is "constraint dependent", and 100 generations are chosen.

IV. Case Study

In this section, the feasibility and rationality of the proposed algorithm are verified using the CitySim data sets [49], and the distribution of natural driving trajectories on the reference path at roundabouts is also analyzed.

In real applications of reference path generation, AVs can obtain road data from the perception system or a high-definition (HD) map. To simplify this step in this study, road data is obtained from [50] (OSM, an HD map format). Considering the page limitation and that non-standard roundabout scenes also cover standard roundabout scenes, the scenario of the #1 entering lane and #5 and #7 exiting lanes of Roundabout(A) in the dataset was chosen to validate the feasibility of the proposed algorithm. Another reason is that these reference path generation scenarios cover two scenarios mentioned in Section II and have enough trajectories to represent the distribution of trajectories at a roundabout. The geometric structure of the roundabout (A) in the CitySim dataset is shown in Fig. 5, and the specific geometric parameters are shown in Table II.

The lane data must be preprocessed before generating reference paths and analyzing the trajectories. First, lane data is optimized according to OSM's standard [51], and the lane center line data of the pre-exit, circulatory, and post-exit sections is extracted. Second, lane center line data based on the World Geodetic System 1984 (WGS84) is converted to the Universal Transverse Mercator (UTM) coordinate system to achieve higher local measurement and spatial analysis accuracy. Finally, trajectory data must be smoothed, and trajectories are classified into different entry-exit pairs according to the area divisions provided by the dataset to prepare for analysis.

Fig. 6 shows the reference path generation results for the two scenarios. Each path is defined by its control points and control polygons. Curvature combs and curvature profiles are the main indicators for evaluating smoothness [52]. The magenta curvature combs visualize the local curvature profile along the path. This indicates that the curvature is continuous and smoothly varying, resulting in a smooth path with no sharp turns. Fig. 6(a) shows the reference path in the scenario of the #1 entering lane and #5 exiting lane of Roundabout(A), where $\alpha_{1,2} = 0.99870$, $\alpha_{2,3} = 0.99637$, $\beta_{1,2} = 15.8472$ and $\beta_{2,3} = -9.4905$. Fig. 6(b) shows the reference path in the scenario of the #1 entering lane and #7 exiting lane of Roundabout(A), where $\alpha_{1,2} = 0.78688$, $\alpha_{2,3} = 0.81987$, $\beta_{1,2} = 2.3239$, $\beta_{2,3} = -4.5521$ and $\Delta = 0.5947$. Fig. 6(b) shows a change in the direction of curvature compared to Fig. 6(a), indicating a more complex path for vehicle entry into the roundabout.

The curvature profile in Fig. 7 more clearly illustrates the G^2 continuity and smoothness of the path generated by different interpolation curve methods. Fig. 7(a) and Fig. 7(b) correspond to the curvature profiles of the reference path for the two scenarios shown in Fig. 6(a) and Fig. 6(b), respectively. The results indicate that, firstly, the reference path based on the Dubins curve cannot generate a segmented path with continuous overall curvature, nor can it accurately characterize the geometric features of a path with variable curvature. Secondly, although the curvature of the segmented path generated by the polynomial curve is continuous, the overall smoothness of the path is poor, especially at the connection of the segmented path. Among them, the polynomial curve in Fig. 7(b) poorly fits the L3 path of the circulatory section with constant curvature, due to the limited expression ability of the polynomial curve and the inability to accurately represent conic curves, such as arcs and ellipses. Finally,

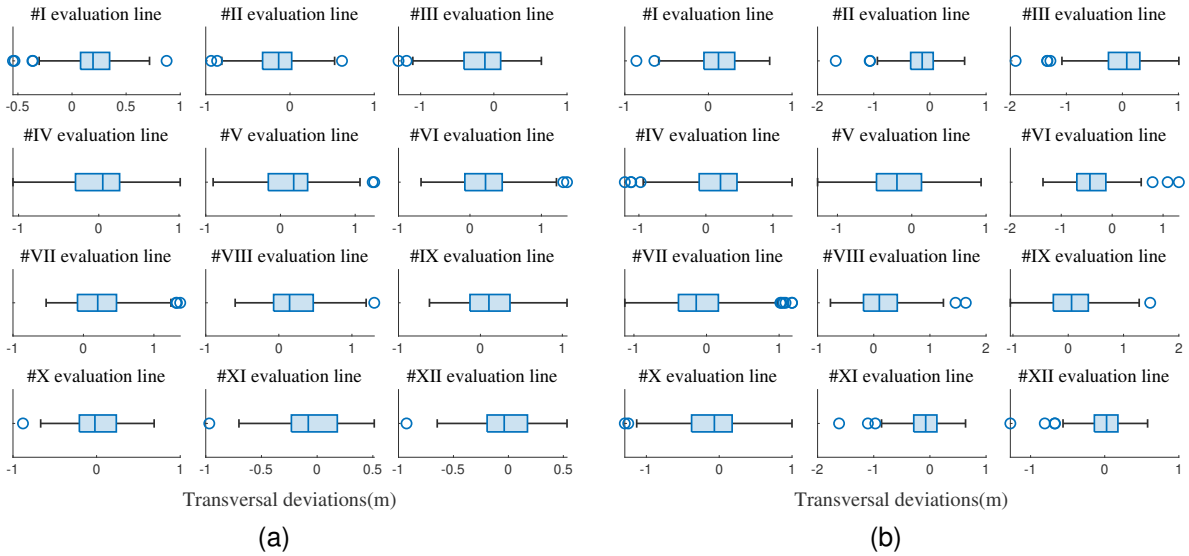

Fig. 9. Box plots of the distributions of the naturalistic driving trajectories on the reference paths of the Lane ID #1-#5 (a) and Lane ID #1-#7 (b) at Roundabout (A).

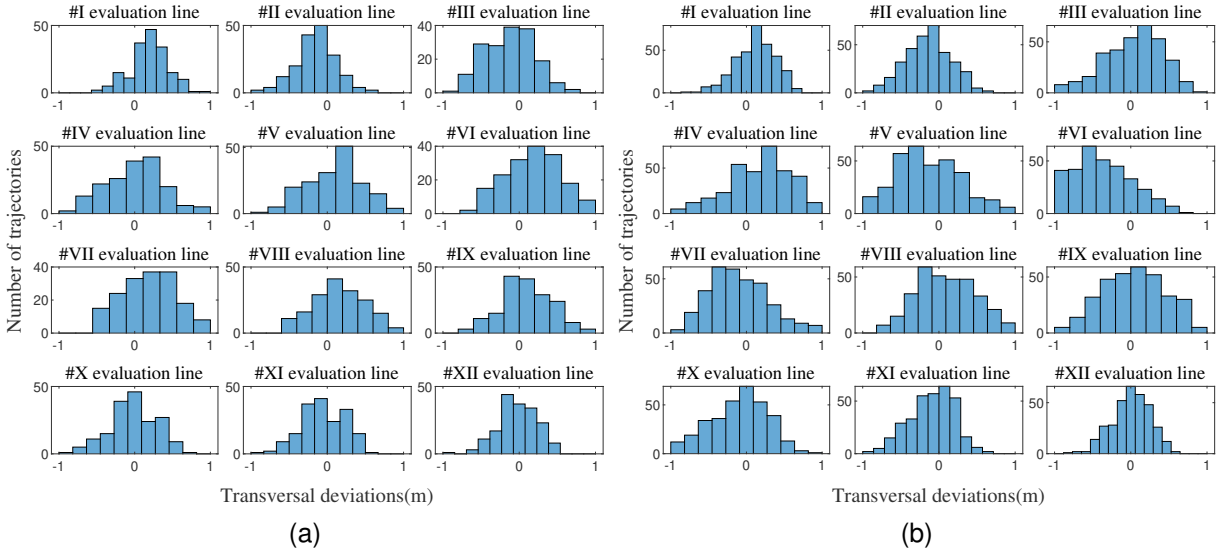

Fig. 10. Histogram of the distributions of the naturalistic driving trajectories on the reference paths of the Lane ID #1-#5 (a) and Lane ID #1-#7 (b) at Roundabout (A).

Bézier curves can better overcome the above difficulties and generate segmented reference paths with continuous curvature and better smoothness. However, it is worth noting that the Bézier curve method still has additional peak curvature. One of the primary reasons is that Bézier curves lack local modification functions, which results in Bézier curves being unable to fully maintain the simplicity of the curve while trying to achieve G^2 continuity with other curves.

Fig. 8 demonstrates the structural features of the roundabout and the distribution of 12 evaluation lines over the reference path, which are evenly spaced according to the geometric features of different scenarios. The evaluation lines are set perpendicular to the entire reference path. This setup of evaluation lines can comprehensively reflect vehicle trajectories at roundabouts and can be used to analyze various factors such as trajectory deviation, comfort, and stability, thereby optimizing and evaluating the driver model for AVs.

The distribution of trajectories is analyzed using box plots in Fig. 9 and histograms in Fig. 10. The box plot analysis method can intuitively compare the distributional differences between two sets of trajectories at roundabouts, providing valuable information for evaluating human driver trajectories and influencing factors. The transversal deviations are the distances between the real and reference paths. Negative transversal deviations represent trajectories to the left of the reference path, and positive values represent trajectories to the right. It can be observed that the overall distribution characteristics reflected in Fig. 9(a) and Fig. 9(b) are somewhat concentrated. The lateral deviations of trajectories are mainly concentrated around zero meters, with relatively small interquartile ranges across evaluation lines, and only a few trajectories presenting relatively large outliers. This indicates that the vehicle trajec-

tories are approximately symmetrically distributed around the reference path. Nonetheless, the credibility and robustness of this conclusion still need further examination, limited by the sample size.

To analyze in detail, and because most trajectories are distributed within one meter, the histogram range in Fig. 10(a) is set to negative and positive one meter. More specifically, the #IV, #V, #VI, and #VII evaluation lines in Fig. 10(a) show left-skewed distributions, meaning the transversal deviations of the right-turn trajectories are shifted to the right of the reference path. Conversely, the #VI and #VII evaluation lines in Fig. 10(b) show right-skewed distributions, meaning the transversal deviations of the left-turn trajectories are shifted to the left of the reference path. These results can be attributed to the tendency of trajectories to move towards the inside of any curved portion of the roundabout, in line with the conclusions mentioned in [41], [53]. Trajectories on the evaluation lines of other parts are essentially normally distributed. The sample of roundabouts used in this study is limited and not fully representative of all roundabouts. However, the results indicate a trend.

V. Conclusion

This paper presents a novel reference path planning algorithm for roundabouts. To cope with the complexity of roundabouts and build a reference path that meets the control and comfort requirements of AVs, the proposed method generates an adaptive G^2 continuity reference path using 5th-order Bézier curves, considering the geometric elements of the roundabout and comfort constraints. Specifically, the reference path generation at roundabouts is divided into six sections: pre-entry, transition, entry, circulation, exit and post-exit. Different scenarios have different section combinations, and the reference path for each section is generated according to the lane marking conditions on both sides. Regarding sections where lane lines exist, the Bézier curves' control points are back-calculated by fitting the discrete points of the lane center line. For sections missing lane markings, the control points are computed using G^2 continuity with other fitting curves. Additionally, to address the problem of determining the merging and diverging points unique to roundabouts, this study presents an appropriate cost function that considers the length and smoothness of the path. Different entry-exit pairs of roundabouts are tested to validate the feasibility of the proposed algorithm. Based on the generated reference path, the distribution of human driver trajectories is analyzed to verify the rationality of the algorithm. The scope of this work focuses solely on the feasibility and rationality of reference path generation for roundabouts using 5th-order Bézier curves.

On one hand, this study establishes a strong foundation for autonomous driving research, particularly in path optimization and tracking control using the Frenet coordinate system. It also serves as preliminary work in trajectory planning. On the other hand, it offers a benchmark for analyzing human driving trajectories in roundabouts and for training and validating human-like driver models for AVs.

Future work will concentrate on enhancing the algorithm's real-time computational efficiency. Offline training of machine learning models can predict optimal merge/diverge point locations, accelerating the path planning process. Curve methods with improved local support, such as B-spline curves or Non-Uniform Rational B-Splines (NURBS), can be explored to enhance path adjustment flexibility and achieve better overall fairness.

References

[1] L. Rodegerdts, "Roundabouts database," 2022. [Online]. Available: https://roundabouts.kittelson.com

[2] F. Patterson, "Cycling and roundabouts: An australian perspective," *Road Transp. Res.*, vol. 19, no. 2, pp. 4–19, 2010.

[3] W. Gardziejczyk and M. Motylewicz, "Noise level in the vicinity of signalized roundabouts," *Transp. Res. D Transp. Environ.*, vol. 46, pp. 128–144, 2016.

[4] R. A. Retting, S. Mandavilli, A. T. McCartt, and E. R. Russell, "Roundabouts, traffic flow and public opinion," *Traffic Eng. Control*, vol. 47, no. 7, pp. 268–272, 2006.

[5] A. Breuer, J.-A. Termöhlen, S. Homoceanu, and T. Fingscheidt, "opendd: A large-scale roundabout drone dataset," in *Proc. IEEE 23rd Int. Conf. ITSC*, Rhodes, Greece, 2020, pp. 1–6.

[6] E. E. M. Chong and R. N. S. Al-Mamari, "Characteristics of drivers' lane choice at large multi-lane roundabout," *Int. J. Integr. Eng.*, vol. 12, no. 9, pp. 176–183, 2020.

[7] Y. Zhang, B. Gao, L. Guo, H. Guo, and H. Chen, "Adaptive decision-making for automated vehicles under roundabout scenarios using optimization embedded reinforcement learning," *IEEE Trans. Neural Networks Learn. Syst.*, vol. 32, no. 12, pp. 5526–5538, 2020.

[8] D. González, J. Pérez, V. Milanés, and F. Nashashibi, "A review of motion planning techniques for automated vehicles," *IEEE Trans. Intell. Transp. Syst.*, vol. 17, no. 4, pp. 1135–1145, 2015.

[9] C. Zhou, B. Huang, and P. Fränti, "A review of motion planning algorithms for intelligent robots," *J. Intell. Manuf.*, vol. 33, no. 2, pp. 387–424, 2022.

[10] H. Fan, F. Zhu, C. Liu, L. Zhang, L. Zhuang, D. Li, W. Zhu, J. Hu, H. Li, and Q. Kong, "Baidu apollo em motion planner," 2018, *arXiv:1807.08048*. [Online]. Available: https://arxiv.org/abs/1807.08048

[11] K. Yoshioka, H. Nakamura, S. Shimokawa, and H. Morita, "Modeling of a novel risk index for evaluating the geometric designs of roundabouts," *Accid. Anal. Prev.*, vol. 145, 2020, art no. 105702.

[12] J. A. Silva and V. Grassi, "Path planning at roundabouts using piecewise linear continuous curvature curves," in *Proc. 2017 LARS and 2017 SBR*, Curitiba, Brazil, 2017, pp. 1–6.

[13] D. González, J. Pérez, and V. Milanés, "Parametric-based path generation for automated vehicles at roundabouts," *Expert Syst. Appl.*, vol. 71, pp. 332–341, 2017.

[14] J. Pérez, V. Milanés, T. De Pedro, and L. Vlacic, "Autonomous driving manoeuvres in urban road traffic environment: a study on roundabouts," *IFAC Proc. Volumes*, vol. 44, no. 1, pp. 13 795–13 800, 2011.

[15] J. L. Rubio-Martín, R. Jurado-Piña, and J. M. Pardillo-Mayora, "Automated identification of fastest vehicle paths at roundabouts," *J. Transp. Eng. A Syst.*, vol. 145, no. 9, 2019, art no. 04019035.

[16] J. Pérez, J. Godoy, J. Villagrá, and E. Onieva, "Trajectory generator for autonomous vehicles in urban environments," in *Proc. 2013 IEEE Int. Conf. Robotics and Automation*, Karlsruhe, Germany, 2013, pp. 409–414.

[17] J. P. Rastelli and M. S. Peñas, "Fuzzy logic steering control of autonomous vehicles inside roundabouts," *Appl. Soft Comput.*, vol. 35, pp. 662–669, 2015.

[18] D. González and J. Pérez, "Control architecture for cybernetic transportation systems in urban environments," in *Proc. 2013 IEEE Intelligent Vehicles Symposium (IV)*, Gold Coast, Australia, 2013, pp. 1119–1124.

[19] R. Lattarulo, L. González, E. Martí, J. Matute, M. Marcano, and J. Pérez, "Urban motion planning framework based on n-bézier curves considering comfort and safety," *J. Adv. Transp*, vol. 2018, no. 1, 2018, art no. 6060924.

[20] C. Hidalgo, R. Lattarulo, J. Pérez, and E. Asua, "Hybrid trajectory planning approach for roundabout merging scenarios," in *Proc. 2019 IEEE ICCVE*, Graz, Austria, 2019, pp. 1–6.

[21] T.-W. Hsu and J.-S. Liu, "Design of smooth path based on the conversion between $\eta 3$ spline and bezier curve," in *Proc. 2020 American Control Conference (ACC)*, Denver, CO, USA, 2020, pp. 3230–3235.

[22] H. Cao and M. Zoldy, "Implementing b-spline path planning method based on roundabout geometry elements," *IEEE Access*, vol. 10, pp. 81 434–81 446, 2022.
[23] Y. Sun, D. Ren, S. Lian, S. Fu, X. Teng, and M. Fan, "Robust path planner for autonomous vehicles on roads with large curvature," *IEEE Rob. Autom. Lett.*, vol. 7, no. 2, pp. 2503–2510, 2022.
[24] K. Yang and S. Sukkarieh, "An analytical continuous-curvature path-smoothing algorithm," *IEEE Trans. Rob.*, vol. 26, no. 3, pp. 561–568, 2010.
[25] B. A. Barsky and T. D. DeRose, *Geometric continuity of parametric curves*. San Francisco: Computer Science Division, University of California San Francisco, CA, 1984.
[26] T. Fraichard and A. Scheuer, "From reeds and shepp's to continuous-curvature paths," *IEEE Trans. Rob.*, vol. 20, no. 6, pp. 1025–1035, 2004.
[27] T. Kito, J. Ota, R. Katsuki, T. Mizuta, T. Arai, T. Ueyama, and T. Nishiyama, "Smooth path planning by using visibility graph-like method," in *Proc. IEEE Int. Conf. Robotics and Automation*, vol. 3, Taipei, China, 2003, pp. 3770–3775.
[28] J.-H. Hwang, R. C. Arkin, and D.-S. Kwon, "Mobile robots at your fingertip: Bezier curve on-line trajectory generation for supervisory control," in *Proc. IEEE/RSJ Int. Conf. IROS 2003*, Las Vegas, NV, USA, 2003, pp. 1444–1449.
[29] B. Song, Z. Wang, and L. Zou, "An improved pso algorithm for smooth path planning of mobile robots using continuous high-degree bezier curve," *Appl. Soft Comput.*, vol. 100, 2021, art no. 106960.
[30] P. E. Koch and K. Wang, "Introduction of b-splines to trajectory planning for robot manipulators," *Model. Ident. Control*, vol. 9, no. 2, pp. 69–80, 1988.
[31] E. Lu, L. Xu, Y. Li, Z. Tang, and Z. Ma, "Modeling of working environment and coverage path planning method of combine harvesters," *Int. J. Agric. Biol. Eng.*, vol. 13, no. 2, pp. 132–137, 2020.
[32] T. Chen, L. Xu, H. S. Ahn, E. Lu, Y. Liu, and R. Xu, "Evaluation of headland turning types of adjacent parallel paths for combine harvesters," *Biosyst. Eng.*, vol. 233, pp. 93–113, 2023.
[33] R. Chai, K. Chen, B. Hua, Y. Lu, Y. Xia, X.-M. Sun, G.-P. Liu, and W. Liang, "A two phases multiobjective trajectory optimization scheme for multi-ugvs in the sight of the first aid scenario," *IEEE Trans. Cybern.*, vol. 54, no. 9, pp. 5078–5091, 2024.
[34] J. Ziegler, P. Bender, T. Dang, and C. Stiller, "Trajectory planning for bertha—a local, continuous method," in *Proc. 2014 IEEE Intelligent Vehicles Symposium*, Dearborn, MI, USA, 2014, pp. 450–457.
[35] Á. Madridano, A. Al-Kaff, D. Martín, and A. De La Escalera, "Trajectory planning for multi-robot systems: Methods and applications," *Expert Syst. Appl.*, vol. 173, 2021, art no. 114660.
[36] R. Chai, H. Niu, J. Carrasco, F. Arvin, H. Yin, and B. Lennox, "Design and experimental validation of deep reinforcement learning-based fast trajectory planning and control for mobile robot in unknown environment," *IEEE Trans. Neural Networks Learn. Syst.*, vol. 35, no. 4, pp. 5778–5792, 2022.
[37] R. Chai, A. Tsourdos, A. Savvaris, S. Chai, Y. Xia, and C. P. Chen, "Design and implementation of deep neural network-based control for automatic parking maneuver process," *IEEE Trans. Neural Networks Learn. Syst.*, vol. 33, no. 4, pp. 1400–1413, 2020.
[38] H. Sun, W. Zhang, R. Yu, and Y. Zhang, "Motion planning for mobile robots—focusing on deep reinforcement learning: A systematic review," *IEEE Access*, vol. 9, pp. 69 061–69 081, 2021.
[39] A. Vinayak, M. A. Zakaria, K. Baarath, and A. P. A. Majeed, "A novel bezier curve control point search algorithm for autonomous navigation using n-order polynomial search with boundary conditions," in *Proc. 2021 IEEE Int. ITSC, Indianapolis*, IN, USA, 2021, pp. 3884–3889.
[40] K. Kawabata, L. Ma, J. Xue, C. Zhu, and N. Zheng, "A path generation for automated vehicle based on bezier curve and via-points," *Rob. Auton. Syst.*, vol. 74, pp. 243–252, 2015.
[41] P. St-Aubin, N. Saunier, L. F. Miranda-Moreno, and K. Ismail, "Use of computer vision data for detailed driver behavior analysis and trajectory interpretation at roundabouts," *Transp. Res. Rec.*, vol. 2389, no. 1, pp. 65–77, 2013.
[42] B. A. Barsky and T. D. DeRose, "Geometric continuity of parametric curves: constructions of geometrically continuous splines," *IEEE Comput. Graphics Appl.*, vol. 10, no. 1, pp. 60–68, 1990.
[43] L. Piegl and W. Tiller, *The NURBS book*. New York, NY: Springer Science & Business Media, 1996.
[44] D. Zeng, Z. Yu, L. Xiong, J. Zhao, P. Zhang, Z. Li, Z. Fu, J. Yao, and Y. Zhou, "A novel robust lane change trajectory planning method for autonomous vehicle," in *Proc. 2019 IEEE Intelligent Vehicles Symposium (IV)*, Paris, France, 2019, pp. 486–493.
[45] E. D. Lambert, R. Romano, and D. Watling, "Optimal smooth paths based on clothoids for car-like vehicles in the presence of obstacles," *Int. J. Control Autom. Syst.*, vol. 19, pp. 2163–2182, 2021.
[46] Y. Jiang, H. Lin, and W. Huang, "Fairing-pia: progressive-iterative approximation for fairing curve and surface generation," *Visual Comput.*, vol. 40, no. 3, pp. 1467–1484, 2024.
[47] F. Caliò, E. Miglio, and M. Rasella, "Curve fairing using integral spline operators," *Int. J. Numer. Methods Biomed. Eng.*, vol. 26, no. 12, pp. 1674–1686, 2010.
[48] A. Wang and G. Zhao, "Curvature variation factor and its application," *Int. J. Wavelets Multiresolut. Inf. Process.*, vol. 15, no. 2, 2017, art no. 1750013.
[49] O. Zheng, M. Abdel-Aty, L. Yue, A. Abdelraouf, Z. Wang, and N. Mahmoud, "Citysim: a drone-based vehicle trajectory dataset for safety-oriented research and digital twins," *Transp. Res. Rec.*, vol. 2678, no. 4, pp. 606–621, 2024.
[50] O. contributors, "Planet dump retrieved from https://planet.osm.org," 2017. [Online]. Available: https://www.openstreetmap.org
[51] O. Wiki, "Tag:junction=roundabout — openstreetmap wiki," 2023. [Online]. Available: https://wiki.openstreetmap.org/w/index.php?title=Tag:junction%3Droundabout&oldid=2542136
[52] G. Farin, "Curvature combs and curvature plots," *Comput. Aided Des.*, vol. 80, pp. 6–8, 2016.
[53] S. Bastos, S. DE MAIA, and J. DA SILVA, "Characterization of trajectories adopted at roundabout crossings," in *Proc. Eur. Transp. Conf.*, Strasburg, France, 2006, pp. 18–20.

Qingyuan Shen received an M.S. degree in vehicle engineering from Jiangsu University, Zhenjiang, China, in 2018 and 2020, where he is currently pursuing a Ph.D. degree in vehicle engineering. Since December 2022, he has been a visiting research student at the Advanced Vehicle Engineering Centre, School of Aerospace, Transport and Manufacturing, Cranfield University, Cranfield, U.K. His research interests include autonomous vehicles, path planning, and decision-making.

Haobin Jiang received a B.S. degree in agricultural mechanization from Nanjing Agricultural University, Nanjing, China, in 1991 and the M.S. and Ph.D. degrees in vehicle engineering from Jiangsu University, Zhenjiang, China, in 1994 and 2000, respectively. From 1994 to 1995, he was a Research Assistant with the Laboratory of Power and Energy, Faculty of Biological Resources, Mie University, Mie, Japan. He joined Jiangsu University, Zhenjiang, China, in 1994, where he is currently a Professor of Vehicle Engineering. He is the Steering Technology Committee Member of the Society of Automotive Engineering of China, the Steering Technology Committee Member of the National Technical Committee of Auto Standardization (China), and the Standing Director of the Society of Automotive Engineering of Jiangsu. His research interests include vehicle dynamic performance analysis and electrical control technology, active safety control techniques and theories of road vehicles, and intelligent transportation technologies.

Aoxue Li received the B.S., M.S. and Ph.D. degrees in vehicle engineering from Jiangsu University, Zhenjiang, China, in 2013, 2016 and 2020, respectively. From August 2018 to August 2019, he was a visiting scholar with the Department of Mechanical Engineering, Michigan State University, East Lansing, MI 48824, USA. He is currently a lecturer at the School of Automotive and Traffic Engineering at Jiangsu University. His research interests include autonomous vehicles, intelligent transportation systems and ADAS technologies.

Marco Cecotti received a Ph.D. degree in electrical engineering from Oxford Brookes University, UK, in 2013. He worked for Tata Motors and Dyson on several automotive projects, focused on vehicle control and driver assistance systems. He is now a Lecturer with the School of Aerospace, Transport and Manufacturing at Cranfield University, UK. His research interests include vehicle trajectory control, path planning, localization and sensor fusion. He is a member of the IEEE.

Chenhui Yin received the B.S. degree in vehicle engineering and the M.S. degree in traffic and transportation engineering from Jiangsu University, Zhenjiang, China, in 2016 and 2019 respectively, where he is currently pursuing the Ph.D. degree. He is also a Ph.D. Researcher at Cranfield University, Bedford, U.K. His research interests include trajectory prediction, human-like decision-making, and trajectory planning of autonomous vehicles.

You Gong received the M.S. degree in automotive engineering from Coventry University, Coventry, U.K., in 2019 and a Ph.D. in the Advanced Vehicle Engineering Centre from Cranfield University, Cranfield, U.K. He is currently a Lecturer in the School of Mechanical and Automotive Engineering at Xiamen University of Technology, Xiamen, China. He has expertise in dynamic system modeling, multi-chemistry battery system topologies, electrical architecture, and robustness multi-objective optimization control. His current research interests include hybrid energy storage systems and transportation system optimization, control algorithms, and real-world applications.

Generating G2 continuity reference paths for autonomous vehicles at roundabouts

Shen, Qingyuan

2025-09

Shen Q, Jiang H, Li A, et al., (2025) Generating G2 continuity reference paths for autonomous vehicles at roundabouts. IEEE Transactions on Intelligent Transportation Systems, Volume 26, Issue 9, September 2025, pp. 13082-13093

https://doi.org/10.1109/tits.2025.3585504